# Sensor-Fault Detection, Isolation and Accommodation for Natural-Gas Pipelines Under Transient Flow

Khadija Shaheen, *Member, IEEE*, Apoorva Chawla, *Member, IEEE*, Ferdinand Evert Uilhoorn, and Pierluigi Salvo Rossi, *Senior Member, IEEE*

***Abstract*—The monitoring of natural gas pipelines is highly dependent on the information provided by different types of sensors. However, sensors are prone to faults, which results in performance degradation and serious hazards such as leaks or explosions. To prevent catastrophic failures and ensure the safe and efficient operation of the pipelines, it is crucial to timely diagnose sensor faults in natural gas pipelines. This paper investigates model-based sensor fault diagnosis techniques in a natural-gas pipeline under transient flow. A fusing architecture based on distributed data fusion is used for implementing the sensor fault detection, isolation, and accommodation (SFDIA) mechanism. The fusing architecture consists of a set of local filters and an information mixer. The local filters estimate the state variables in parallel, which are subsequently transferred to the information mixer to evaluate the sensor faults and compute fault-free state estimates. In this paper, three different types of fusing filters, namely based on the ensemble Kalman filter (EnKF), fusing unscented Kalman filter (UKF), and fusing extended Kalman filter (EKF) are investigated for fault diagnosis. Results demonstrate that all three filters can successfully detect, isolate, and accommodate sensor faults.**

***Index Terms*—Data fusion, ensemble Kalman filter, extended Kalman filter, fault diagnosis, model-based technique, natural-gas pipelines, sensor validation, transient flow, unscented Kalman filter.**

## I. Introduction

NATURAL gas is extensively utilized in household and commercial settings, making safety requirements for pipelines extremely relevant. Leakage monitoring techniques play a vital part in safe system development and operation [1], and are also critical in various industrial scenarios [2]. Late or missed detection of leakages may have dangerous consequences such as explosions, therefore the development of efficient, robust, and reliable monitoring systems is crucial. Several monitoring systems for urban gas pipelines have been recently deployed to detect leaks in gas pipelines and underground areas [3], [4]. However, most works have focused on leak detection in steady-state flow [5], [6], [7], [8], while transient-flow modeling that depicts the actual flow of fluids in pipelines has gained attention only recently [9].

With the growth of smart cities and digital twins,[1] pipeline monitoring systems are expected to be an integral part of these frameworks, particularly for safety-critical applications [10]. Moreover, sensors play a crucial role in urban gas-pipeline monitoring systems and ensure the effective functioning of digital twins for urban pipelines, since their status directly impacts the security and reliability of the overall system. Unfortunately, sensors are susceptible to damage during their operation due to harsh environmental conditions which include sludge, decaying materials, and floodwater [11].

Sensor-fault detection, isolation and accommodation (SFDIA) has proven to be an effective and necessary technique for handling sensor faults in safety-critical systems. The main objectives of SFDIA are to notify users when faults have occurred, identify their location and structure, and possibly replace the corrupted information such that the system can keep operating. In general, most SFDIA techniques can be divided into model-based methods and data-driven methods. In recent years, data-driven fault-diagnosis methods have received interest due to their versatility and large availability of data in some applications [12], [13], [14], [15]. However, they are more difficult to use in industrial scenarios because a large amount of data might not be available (e.g. due to excessive required costs). Differently, model-based techniques are not limited by data availability and, given that the system model is sufficiently accurate, they exhibit interesting scaling and generalization properties. Additionally, they are easy to interpret, as they usually rely on physics-based information, thus better prepared for explainability requirements.

Manuscript received 20 November 2023; accepted 6 March 2024. Date of publication 13 March 2024; date of current version 26 March 2024. This work was supported by the Research Council of Norway through the Project SIGNIFY within the IKTPLUSS Framework under Project 311902. Part of this work has been submitted to the IEEE Sensors Conference 2023, Vienna, Austria. The associate editor coordinating the review of this manuscript and approving it for publication was Dr. Lifeng Lai. *(Corresponding author: Khadija Shaheen.)*

Khadija Shaheen and Apoorva Chawla are with the Department of Electronic Systems, Norwegian University of Science and Technology, 7491 Trondheim, Norway (e-mail: shaheen.khadija@ntnu.no; apoorva.chawla@ntnu.no).

Ferdinand Evert Uilhoorn is with the Department of Gas Engineering, Warsaw University of Technology, 00-661 Warsaw, Poland (e-mail: ferdinand.uilhoorn@pw.edu.pl).

Pierluigi Salvo Rossi is with the Department of Electronic Systems, Norwegian University of Science and Technology, 7491 Trondheim, Norway, and also with the Department of Gas Technology, SINTEF Energy Research, 7491 Trondheim, Norway (e-mail: salvorossi@ieee.org).

Digital Object Identifier 10.1109/TSIPN.2024.3377134

[1] A digital twin is a digital representation of a physical system, equipped with advanced analytics and driven by real-time sensor data.

Model-based methods work by analyzing the residual signal defined as the difference between the outputs of a computational model and real-world measurements. Two different architectures are usually considered in model-based fault diagnosis for large-size distributed systems: centralized and distributed. The centralized architecture offers high accuracy but requires large computational costs which may limit real-time implementation in the case of a large number of sensors [16], [17]. In contrast, distributed architectures exploit data fusion, i.e. they combine information from multiple sensors, to improve decision-making and reduce the overall computational burden [18], [19], [20], [21], [22]. One of the most effective model-based approaches exploits the Kalman filter (KF) [23], and several generalizations were proposed to deal with nonlinear systems, including the extended KF (EKF) [24], the unscented KF (UKF) [25], the ensemble KF (EnKF) [26] and the cubature KF (CKF) [27]. Also, various frameworks for distributed implementations of the KF have been recently investigated [28].

Distributed data-fusion architectures based on (variants of) KF can also be exploited for fault diagnosis in large-size networked systems. In [29], sensor fusion is utilized for fault diagnosis of multi-channel estimation, however, fault isolation is not taken into account and the system is not suitable for nonlinear systems. Similarly, in [30] a fault-detection method specific for micro-electro-mechanical systems is developed without isolation capabilities. Other works (e.g. [31], [32], and [33]) focus on multi-sensor data fusion for detecting both hardware and software faults. These approaches employ a redundancy-based approach (duplication/comparison) for fault diagnosis, where two sensors are used for estimating one parameter, still their complexity increases considerably when dealing with multiple faults. Centralized and distributed multi-sensor architectures with data fusion based on adaptive EKFs for detecting both sensor and process faults were discussed in [34]. The centralized architecture (with a single filter combining all raw data from different sensors) exhibits high estimation accuracy, but low robustness against sensor faults. The distributed architecture (with a bank of local filters; one per sensor) showed limited capability in detecting multiple sensor faults and dealing with severe non-linearity. In [35], a Wasserstein average consensus classification-based fusion algorithm is proposed to address the problem of faulty sensors. Local filters share information with their neighbors and use clustering algorithms to identify trusted and untrusted local estimates. However, this approach is limited to linear systems with at least half of the sensors being reliable. In [36], an approach for distributed secure linear state estimation using reachability analysis and distributed diffusion KF is discussed. Reachability analysis is used to monitor the deviation of local estimation and provide secure information sharing among nodes. A distributed sensor deception attack and estimation for a class of platoon-based connected vehicles is discussed in [37]. Local state information is extracted via a distributed KF and residuals are processed via a modified generalized likelihood ratio (GLR) algorithm that detects the attacks. However, techniques in both [36] and [37] are designed for linear systems only.

A sensor-fusion scheme for nonlinear systems based on multiple KFs, each tailored for a specific defect, was proposed in [38], but showed significant limitations in terms of computational cost. A sensor-fusion method based on UKF was proposed for monitoring a gas turbine engine in [39]: four local filter combinations were considered (given the sensors deployed on the gas turbine), however, the method lacks generalization and is unable to correctly isolate the defective sensor(s). A UKF-based sensor-fusion system was also developed for microgrid applications, where the number of local filters can be adapted to deal with an arbitrary number of sensors, although the method has not been tested in large-scale distributed systems [40]. Trade-offs between performance and scalability have been analyzed in [41], [42], [43] comparing distributed and centralized architectures. The distributed nature along with a large number of subsystems in natural-gas pipelines points towards distributed fault-detection methods [44], [45], however, to the best of our knowledge, a distributed framework exploiting a model-based approach for SFDIA in pipelines does not exist.

In this paper, we propose a model-based SFDIA system for natural-gas pipelines under transient flow exploiting a KF-based sensor-fusion architecture. The system collects information from different distributed sensors and processes it via several local filters. The outputs from local filters are combined to provide a robust SFDIA and improve decision-making in the monitoring systems. Also, the computational burden of the system is distributed over different local filters which can run in parallel. Additionally, this study introduces SFDIA for a highly nonlinear and intricate transient flow model described by partial differential equations (PDEs). Traditionally, prevailing methods have overlooked the challenges posed by utilizing large-scale PDE systems. Furthermore, existing approaches rely on simplistic models that fail to encompass the diverse range of large-scale dynamics observed in real-world complex processes. In contrast, our flow model incorporates highly nonlinear thermodynamic properties and extensive spatio-temporal dynamics at a large scale. Notably, there is currently no existing SFDIA tailored for such models. To tackle these challenges, we propose a sensor-fusion strategy for SFDIA using a transient flow model. Moreover, we presented and evaluated our suggested architecture with three different local filters (EnKF, UKF, EKF). Given the highly nonlinear and large-scale nature of our system, the fusing architecture employing EnKF and UKF has specifically demonstrated high performance. Our work is based on [40], where the fusing architecture with only UKF has been investigated for micro-grid systems. In contrast, we investigated the fusing architecture for a highly nonlinear and complex flow model in the context of fault diagnosis. Table I contrasts the key features of the proposed work with those of the closely related works reviewed above. More specifically, the main contributions of this work are listed below.

- A model-based SFDIA architecture, based on a distributed FK approach, for natural-gas pipelines under transient flow is proposed and discussed for the first time;
- A transient flow model is thoroughly discussed along with its numerical solution with a focus on SFDIA application (while commonly it is linked to leakage detection);

TABLE I
COMPARISON OF THE EXISTING SENSOR FAULT DIAGNOSIS METHODS WITH OUR PROPOSED TECHNIQUE

| Works | Filter type | Applications | High-dimensional system | Non-linearity | Transient | Differential equation | Weak random faults | Fault detection | Fault accommodation |
|---|---|---|---|---|---|---|---|---|---|
| [34] | EKF | Stirred tank reactor | ✗ | ↓ Low | ✗ | ODE | ✗ | ✓ | ✓ |
| [31],[32] | KF | Navigation system | ✗ | ↓ Low | ✗ | ODE | ✗ | ✓ | ✓ |
| [38] | KF | Navigation system | ✗ | ↓ Low | ✗ | ODE | ✗ | ✓ | ✓ |
| [39] | EKF, UKF | Gas turbine engine | ✗ | ↓ Low | ✗ | ODE | ✗ | ✓ | ✓ |
| [40] | UKF | Micro grid | ✗ | ↓ Low | ✗ | ODE | ✗ | ✓ | ✓ |
| [46] | Observer | Hot strip mill | ✗ | ↓ Low | ✓ | PDE | ✗ | ✓ | ✗ |
| Proposed | EnKF,UKF,EnKF | Natural gas pipeline | ✓ | ↑ High | ✓ | PDE | ✓ | ✓ | ✓ |

- A generalized sensor-fusion strategy for SFDIA is presented with the performance assessment shown for three types of local filters (EnKF, UKF, EKF);
- The effectiveness of the proposed architecture is assessed using simulated nonlinear spatio-temporal data coupled with synthetically-generated faults (we focus on two relevant types of faults, namely *bias faults* and *drift faults*), with results shown in terms of probability of detection, probability of false alarm, and accuracy under different scenarios.

The remainder of the paper is organized as follows. In Section II, the transient flow model is presented in detail. Section III discusses the sensor-fusion strategy for SFDIA based on different types of local filters and Section IV explains the data generation process. In Section V, numerical results are compared and discussed to evaluate the performance of the proposed SFDIA methods. Finally, Section VI provides some concluding remarks and future directions.

*Notation:* Lower-case (resp. upper-case) bold letters denote column vectors and matrices; $(\cdot)^T$ denotes the transpose operator; $(\boldsymbol{A})_j$ denotes the $j$th column of the matrix $\boldsymbol{A}$.

## II. TRANSIENT-FLOW MODEL

### A. Partial Differential Equations

The mathematical model for natural gas in pipelines experiencing transient flow can be characterized by a first-order quasilinear non-homogeneous hyperbolic system of PDEs [8]. Applying the laws of conservation of mass, momentum, and energy, the system of PDEs can be written as

$$\frac{\partial \rho}{\partial t} + \frac{\partial}{\partial s}(\rho \nu) = 0 \,, \tag{1}$$

$$\rho \frac{\partial \nu}{\partial t} + \frac{\partial p}{\partial s} + \rho \nu \frac{\partial \nu}{\partial s} = -\frac{w}{A} - \rho g \sin\theta \,, \tag{2}$$

$$\rho \left( \frac{\partial h}{\partial t} + \nu \frac{\partial h}{\partial s} \right) - \frac{\partial p}{\partial t} - \nu \frac{\partial p}{\partial s} = \frac{q + w\nu}{A} \,, \tag{3}$$

where $t$ and $s$ denote time and space variables and the quantities $p$, $\rho$, $\nu$, $w$, $A$, $h$, $g$, $\theta$ and $q$ represent the pressure, density, velocity, frictional force per unit length of pipe, cross-sectional area, specific enthalpy, gravitational acceleration, angle of inclination, and heat flow into the pipe per unit length and time, respectively. The spatio-temporal domain is defined as $\Omega = \{(s,t) : 0 \le s \le L, 0 \le t \le t_f\}$, where $L$ is the pipeline length and $t_f$ is the time span. Using the real gas equation of state $p = z\rho RT$ (where $z$ is the gas compressibility factor, $R$ is the ideal gas constant, and $T$ is the temperature), the thermodynamic identity [47] is given by

$$dh = C_p dT + \left( \frac{T}{\rho} \left( \frac{\partial \rho}{\partial T} \right)_p + 1 \right) \frac{dp}{\rho} \,, \tag{4}$$

where $C_p$ is the specific heat at constant pressure, (1) to (3) can be rewritten with pressure, velocity, and temperature as the dependent variables and are given in [48]. Further, it is convenient to express the governing system of hyperbolic PDEs in terms of pressure, flow, and temperature, which can be written in compact form as

$$\frac{\partial \boldsymbol{x}}{\partial t} + \boldsymbol{A}(\boldsymbol{x}) \frac{\partial \boldsymbol{x}}{\partial s} + \boldsymbol{\zeta}(\boldsymbol{x}) = 0 \,, \tag{5}$$

where $\boldsymbol{x} = [p, \dot{m}, T]^T$. For $\theta = \pi$, the coefficient matrix $\boldsymbol{A}(\boldsymbol{x}) \in \mathbb{R}^{3\times 3}$ is defined in (6) shown at the bottom of the next page and the vector $\boldsymbol{\zeta}(\boldsymbol{x}) \in \mathbb{R}^{3\times 1}$ is given as

$$\boldsymbol{\zeta}(\boldsymbol{x}) = \left[ -\frac{a_s^2 \alpha_1 (Aqp + RT\dot{m}wz)}{A^2 T C_p p} \quad w \quad -\frac{a_s^2 \alpha_2 (Aqp + RT\dot{m}wz)}{A^2 C_p p^2} \right]^T \,,$$

with $\alpha_1 = 1 + \frac{T}{z}\left(\frac{\partial z}{\partial T}\right)_p$ and $\alpha_2 = 1 - \frac{p}{z}\left(\frac{\partial z}{\partial p}\right)_T$. The isentropic wave speed is defined as $a_s = (\partial p / \partial \rho)_s^{1/2}$, where

$$\left( \frac{\partial p}{\partial \rho} \right)_s = \left[ \frac{\rho}{p} \left( 1 - \frac{p}{z} \left( \frac{\partial z}{\partial p} \right)_T - \frac{p}{\rho C_p T} \left( 1 + \frac{T}{z} \left( \frac{\partial z}{\partial T} \right)_p \right)^2 \right) \right]^{-1} \,.$$

The frictional force per unit length $w$ can be expressed as $w = \frac{1}{8} f \rho v |v| \pi d$, where $d$ is the diameter, and the friction factor $f$ is computed using the Colebrook–White equation [49]

$$\frac{1}{\sqrt{f}} = -2\log\left( \frac{\epsilon}{3.7\, d} + \frac{2.51}{Re\sqrt{f}} \right) \,,$$

where $\epsilon$ is the roughness and $Re$ is the Reynolds number. The heat transfer between the natural gas and its surroundings per unit length and time is given as $q = -\pi d U (T - T_s)$, where $T_s$ is the ambient temperature and $U$ is the overall heat transfer coefficient. The thermodynamic and transport properties $C_p$ and $z$ are fitted to the values calculated by GERG-2004 [8], [50].

### B. Method of Lines

An effective method to solve transient models involving PDEs is the method of lines [51], which is based on spatial discretization. A 5-point, fourth-order finite difference method is employed to spatially discretize the system of PDEs in (5) to obtain a set of ordinary differential equations (ODEs). The error of this approximation is $\mathcal{O}(\Delta s^4)$. After this conversion, the state vector $\boldsymbol{x}$ can be formulated as

$$\boldsymbol{x}(t) = [p_1(t), \ldots, p_i(t), \ldots, p_n(t), \dot{m}_1(t), \ldots, \dot{m}_i(t), \ldots, \dot{m}_n(t), T_1(t), \ldots, T_i(t), \ldots, T_n(t)]^T , \quad (7)$$

and the system of ODEs can be expressed as

$$\frac{d\boldsymbol{x}(t)}{dt} = \boldsymbol{A}(\boldsymbol{x})\boldsymbol{D}\boldsymbol{x}(t) - \boldsymbol{\zeta}(\boldsymbol{x}, t) \triangleq \boldsymbol{\varphi}(t, \boldsymbol{x}(t)) , \quad (8)$$

where $\boldsymbol{\zeta}(\boldsymbol{x}, t) \in \mathbb{R}^{3n\times 1}$ is the assembled column vector of $\boldsymbol{\zeta}(\boldsymbol{x})$ and $\boldsymbol{A}(\boldsymbol{x}) \in \mathbb{R}^{3n\times 3n}$ is the assembled matrix. The computational matrix is defined as

$$\boldsymbol{D} = -\frac{1}{12\Delta s}\begin{bmatrix} -25 & 48 & -36 & 16 & -3 & \cdots & 0 \\ -3 & -10 & 18 & -6 & 1 & \cdots & 0 \\ 1 & -8 & 0 & 8 & -1 & \cdots & 0 \\ \vdots & \ddots & \ddots & \ddots & \ddots & \ddots & \vdots \\ 0 & \cdots & 1 & -8 & 0 & 8 & -1 \\ 0 & \cdots & -1 & 6 & -18 & 10 & 3 \\ 0 & \cdots & 3 & -16 & 36 & -48 & 25 \end{bmatrix} .$$

The fourth-order Runge-Kutta method (RK4) is utilized to solve the system of ODEs in (8) due to its effectiveness and simplicity. The discretized equations with fixed time step can be characterized as a state-space model and its solution (advanced in time $t_k$) can be expressed as

$$\boldsymbol{x}_{k+1} = \boldsymbol{x}_k + \frac{\Delta t}{6}(\boldsymbol{k}_1 + 2\boldsymbol{k}_2 + 2\boldsymbol{k}_3 + \boldsymbol{k}_4) ,$$

with

$$\begin{aligned} \boldsymbol{k}_1 &= \boldsymbol{\varphi}(\boldsymbol{x}_k, t_k) , \\ \boldsymbol{k}_2 &= \boldsymbol{\varphi}\left(\boldsymbol{x}_k + \frac{\Delta t}{2}\boldsymbol{k}_1, t_k + \frac{\Delta t}{2}\right) , \\ \boldsymbol{k}_3 &= \boldsymbol{\varphi}\left(\boldsymbol{x}_k + \frac{\Delta t}{2}\boldsymbol{k}_2, t_k + \frac{\Delta t}{2}\right) , \\ \boldsymbol{k}_4 &= \boldsymbol{\varphi}\left(\boldsymbol{x}_k + \Delta t\boldsymbol{k}_3, t_k + \Delta t\right) , \end{aligned}$$

where $\boldsymbol{x}_k = \boldsymbol{x}(t_k)$ and $t_k = k(\Delta t)$.

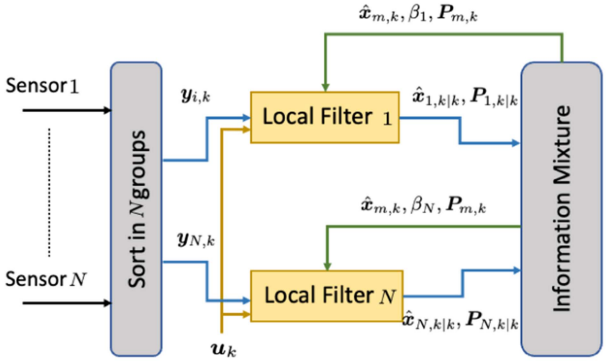


Fig. 1. Data-fusion architecture.

Further, the Courant-Friedrichs-Lewy (CFL) [52] condition should be satisfied to guarantee numerical stability, i.e.

$$\frac{\Delta t}{\Delta s} \leq \frac{1}{|\nu| + a_s} . \quad (9)$$

## III. Sensor Fusion for Fault Diagnosis

### A. System Architecture

We consider a data-fusion architecture for state estimation based on the integration of several local filters and an information mixture. The architecture offers appealing performance for fault diagnosis and isolation while decentralizing the computational load from one master filter to numerous local filters. The schematic diagram of the data-fusion architecture is shown in Fig. 1. The architecture mainly operates with four stages: first, the sensor measurements are grouped into various subsets of measurements; second, all local filters simultaneously determine the state vector estimate and covariance; third, the global state estimate and covariance are evaluated in the information mixture using the state estimates of the local filters; finally, the local filters are updated with the global parameters.

The discrete-time process and measurement models for the $i$th local filter can be expressed by the following equations

$$\boldsymbol{x}_{i,k} = \boldsymbol{f}_i(\boldsymbol{x}_{i,k-1}, \boldsymbol{u}_{k-1}) + \boldsymbol{v}_{i,k} , \quad (10)$$

$$\boldsymbol{y}_{i,k} = \boldsymbol{h}_i(\boldsymbol{x}_{i,k}, \boldsymbol{u}_k) + \boldsymbol{n}_{i,k} , \quad (11)$$

where the nonlinear mappings $\boldsymbol{f}_i(\cdot,\cdot) : \mathbb{R}^{n_x} \times \mathbb{R}^{n_u} \to \mathbb{R}^{n_x}$ and $\boldsymbol{h}_i(\cdot,\cdot) : \mathbb{R}^{n_x} \times \mathbb{R}^{n_u} \to \mathbb{R}^{n_y}$ represent the process and measurement models at the $i$th local filter, respectively, $\boldsymbol{y}_{i,k} \in \mathbb{R}^{n_y\times 1}$ is the filter output, $\boldsymbol{v}_{i,k} \in \mathbb{R}^{n_x\times 1}$ and $\boldsymbol{n}_{i,k} \in \mathbb{R}^{n_y\times 1}$ denote the process and measurement noises which are assumed to be zero-mean Gaussian with covariance matrices $\boldsymbol{Q}_{i,k} \in \mathbb{R}^{n_x\times n_x}$ and $\boldsymbol{R}_{i,k} \in \mathbb{R}^{n_y\times n_y}$, respectively. Although the noise in a data-fusion architecture is known to be correlated [53], we will assume uncorrelated noise. We assume that the number of

$$\boldsymbol{A}(\boldsymbol{x}) = \begin{bmatrix} -\frac{\dot{m}(a_s^2\alpha_2 - RTz)}{Ap} & \frac{a_s^2}{A} & \frac{a_s^2\dot{m}\alpha_1}{AT} \\ A - \frac{a_s^2\alpha_2^2 C_p\dot{m}^2 - Ra_s^2\alpha_1^2\alpha_2\dot{m}^2 z}{AC_p p^2} & \frac{\dot{m}(\alpha_2 C_p a_s^2 - Rza_s^2\alpha_1^2 + RTC_p z)}{AC_p p} & \frac{a_s^2\alpha_1\dot{m}^2(\alpha_2 C_p - R\alpha_1^2 z)}{ATC_p p} \\ -\frac{RTa_s^2\alpha_1\alpha_2\dot{m}z}{AC_p p^2} & \frac{RTa_s^2\alpha_1 z}{AC_p p} & \frac{R\dot{m}z(a_s^2\alpha_1^2 + TC_p)}{AC_p p} \end{bmatrix} \quad (6)$$

local filters is equal to the number of sensors, namely $N$. The state vector $\boldsymbol{x}_{i,k} \in \mathbb{R}^{n_x \times 1}$ is defined as

$$\boldsymbol{x}_{i,k} = [p_1(k), \ldots, p_n(k), \dot{m}_1(k), \ldots, \dot{m}_n(k), T_1(k), \ldots, T_n(k)]^T . \tag{12}$$

The input vector $\boldsymbol{u}_{k-1} \in \mathbb{R}^{n_u \times 1}$ is obtained using the initial and boundary conditions and is defined as $\boldsymbol{u}_{k-1} = [\boldsymbol{u}_{in}^T \boldsymbol{u}_{bc,k-1}^T]^T$. Next we discuss the data-fusion architecture based on the process and measurement models in (10) and (11).

### B. Fusion Strategy for Fault-Free System

The four steps of the algorithm implementing the data-fusion architecture are described below.

*Step 1:* The local state estimate $\hat{\boldsymbol{x}}_{i,0|0}$ and the local covariance matrix $\boldsymbol{P}_{i,0|0} \in \mathbb{R}^{n_x \times n_x}$ of all the local filters are initialized depending on the specific use case.

*Step 2:* The time and measurement updates are performed depending on the type of local filters. In this paper, we considered three types of local filters: EKF, EnKF, and UKF. The local filters are explicitly discussed in Sections III-C1, III-C2, and III-C3, respectively.

*Step 3:* The global parameters, i.e. the global state estimate $\hat{\boldsymbol{x}}_{m,k}$, the global state covariance matrix $\boldsymbol{P}_{m,k}$ and the global process noise covariance matrix $\boldsymbol{Q}_{m,k}$, are evaluated in the information mixture using the local state estimate $\hat{\boldsymbol{x}}_{i,k|k}$, the state covariance matrix $\boldsymbol{P}_{i,k|k}$ and the process noise covariance matrix $\boldsymbol{Q}_{i,k}$, as follows

$$\boldsymbol{Q}_{m,k} = \left( \sum_{i=1}^{N} \boldsymbol{Q}_{i,k}^{-1} \right)^{-1}, \quad \boldsymbol{P}_{m,k} = \left( \sum_{i=1}^{N} \boldsymbol{P}_{i,k|k}^{-1} \right)^{-1},$$

$$\hat{\boldsymbol{x}}_{m,k} = \boldsymbol{P}_{m,k} \sum_{i=1}^{N} \boldsymbol{P}_{i,k|k}^{-1} \hat{\boldsymbol{x}}_{i,k|k} .$$

*Step 4:* The global estimates obtained in Step 3 are subsequently utilized to update all the local filters. The local state estimate $\hat{\boldsymbol{x}}_{i,k|k}$, the state covariance matrix $\boldsymbol{P}_{i,k|k}$ and the process noise covariance matrix $\boldsymbol{Q}_{i,k}$ can be obtained from the global parameters as follows

$$\boldsymbol{Q}_{i,k} = \beta_i \boldsymbol{Q}_{m,k} , \quad \boldsymbol{P}_{i,k|k} = \beta_i \boldsymbol{P}_{m,k} , \quad \sum_{i=1}^{N} \beta_i = 1 ,$$

$$\hat{\boldsymbol{x}}_{i,k|k} = \hat{\boldsymbol{x}}_{m,k} ,$$

where $\beta_i$ is an information distribution factor weighting the $i$th local filter.

The detailed block diagram of the local filter and the information mixture is shown in Fig. 2. Further, the estimates of each local filter (time update and measurement update) are independent of the estimates of other local filters. The architecture of the local filters is discussed in the next subsection.

### C. Local-Filter Structure

We describe the measurement and time updates for the three considered types of local filters: EKF, EnKF, and UKF. They represent relevant KF-based techniques capable to handle nonlinear systems.

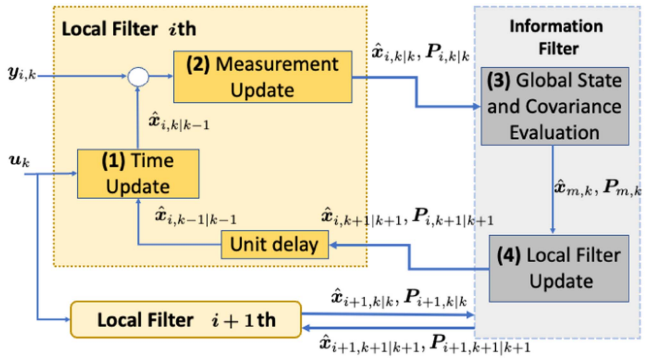


Fig. 2. Data-fusion architecture depicting a single local filter and information mixture.

*1) Extended Kalman Filter:* The EKF is the most widely-used Bayesian estimation technique for nonlinear systems. It is based on the linearization of the nonlinear process and measurement models around the most recent state estimate.

Using the first-order Taylor series expansion about the state estimate $\hat{\boldsymbol{x}}_{i,k-1|k-1}$, the *a priori* state estimate and covariance are evaluated as

$$\hat{\boldsymbol{x}}_{i,k|k-1} = \boldsymbol{f}_i(\hat{\boldsymbol{x}}_{i,k-1|k-1}, \boldsymbol{u}_{k-1}) ,$$

$$\boldsymbol{P}_{i,k|k-1} = \boldsymbol{F}_{i,k} \boldsymbol{P}_{i,k-1|k-1} \boldsymbol{F}_{i,k}^T + \boldsymbol{Q}_{i,k} ,$$

while the predicted mean and covariance of $\boldsymbol{y}_{i,k}$ and the cross-covariance between $\boldsymbol{x}_{i,k}$ and $\boldsymbol{y}_{i,k}$ are evaluated as

$$\hat{\boldsymbol{y}}_{i,k|k-1} = \boldsymbol{h}_i(\hat{\boldsymbol{x}}_{i,k|k-1}, \boldsymbol{u}_k) ,$$

$$\boldsymbol{P}_{i,k|k-1}^{y} = \boldsymbol{H}_{i,k} \boldsymbol{P}_{i,k|k-1} \boldsymbol{H}_{i,k}^T + \boldsymbol{R}_{i,k} ,$$

$$\boldsymbol{P}_{i,k|k-1}^{xy} = \boldsymbol{P}_{i,k|k-1} \boldsymbol{H}_{i,k}^T ,$$

where $\boldsymbol{F}_{i,k}$ and $\boldsymbol{H}_{i,k}$ are the Jacobian matrices of the nonlinear functions $\boldsymbol{f}_i(\cdot,\cdot)$ and $\boldsymbol{h}_i(\cdot,\cdot)$, respectively defined in (10) and (11), computed as

$$\boldsymbol{F}_{i,k} = \left. \frac{\partial \boldsymbol{f}_i}{\partial \boldsymbol{x}} \right|_{\hat{\boldsymbol{x}}_{i,k-1|k-1}}, \qquad \boldsymbol{H}_{i,k} = \left. \frac{\partial \boldsymbol{h}_i}{\partial \boldsymbol{x}} \right|_{\hat{\boldsymbol{x}}_{i,k|k-1}} .$$

Using the above expressions, the *a posteriori* state estimate and the Kalman gain are

$$\hat{\boldsymbol{x}}_{i,k|k} = \hat{\boldsymbol{x}}_{i,k|k-1} + \boldsymbol{K}_{i,k}(\boldsymbol{y}_{i,k} - \hat{\boldsymbol{y}}_{i,k|k-1}) , \tag{13}$$

$$\boldsymbol{K}_{i,k} = \boldsymbol{P}_{i,k|k-1}^{xy} (\boldsymbol{P}_{i,k|k-1}^{y})^{-1} . \tag{14}$$

Also, the covariance is given as

$$\boldsymbol{P}_{i,k|k} = (\boldsymbol{I} - \boldsymbol{K}_{i,k} \boldsymbol{H}_{i,k}) \boldsymbol{P}_{i,k|k-1} .$$

The time update and the measurement update of the EKF are summarized as follows.

*Time Update:*

$$\hat{\boldsymbol{x}}_{i,k|k-1} = \boldsymbol{f}_i(\hat{\boldsymbol{x}}_{i,k-1|k-1}, \boldsymbol{u}_{k-1}),$$

$$\boldsymbol{P}_{i,k|k-1} = \boldsymbol{F}_{i,k} \boldsymbol{P}_{i,k-1|k-1} \boldsymbol{F}_{i,k}^T + \boldsymbol{Q}_{i,k},$$

$$\hat{\boldsymbol{y}}_{i,k|k-1} = \boldsymbol{h}_i(\hat{\boldsymbol{x}}_{i,k|k-1}, \boldsymbol{u}_k) \ .$$

*Measurement Update:*

$$\boldsymbol{K}_{i,k} = \boldsymbol{P}_{i,k|k-1}\boldsymbol{H}_{i,k}^T \left(\boldsymbol{H}_{i,k}\boldsymbol{P}_{i,k|k-1}\boldsymbol{H}_{i,k}^T + \boldsymbol{R}_{i,k}\right)^{-1},$$

$$\hat{\boldsymbol{x}}_{i,k|k} = \hat{\boldsymbol{x}}_{i,k|k-1} + \boldsymbol{K}_{i,k}(\boldsymbol{y}_{i,k} - \hat{\boldsymbol{y}}_{i,k|k-1}) \ ,$$

$$\boldsymbol{P}_{i,k|k} = (\boldsymbol{I} - \boldsymbol{K}_{i,k}\boldsymbol{H}_{i,k})\,\boldsymbol{P}_{i,k|k-1}.$$

*2) Ensemble Kalman Filter:* The EnKF is a Monte Carlo approximation of the KF, which is particularly useful for state estimation in high-dimensional nonlinear systems. This statistical method maintains an ensemble representing the conditional distribution of a random state vector given the measurement set. The state estimate is generated from the sample mean and covariance of the ensemble.

Let us consider an ensemble of samples, $\{\hat{\boldsymbol{x}}^{(j)}_{i,k-1|k-1}, 1 \leq j \leq N_e\}$, drawn from $p(\boldsymbol{x}_{i,k-1}|\mathbb{Y}_{i,k-1})$, where $\mathbb{Y}_{i,k-1} = \{\boldsymbol{y}_{i,1}, \boldsymbol{y}_{i,2}, \ldots, \boldsymbol{y}_{i,k-1}\}$ and $N_e$ is the ensemble size, to approximately represent the considered PDF. Similarly, an ensemble of samples $\{\boldsymbol{v}^{(j)}_{i,k}, 1 \leq j \leq N_e\}$, drawn from the Gaussian distribution $\mathcal{N}(\boldsymbol{0}, \boldsymbol{Q}_{i,k})$, represents the process noise $\boldsymbol{v}_{i,k}$. Then, the *apriori* ensemble $\{\hat{\boldsymbol{x}}^{(j)}_{i,k|k-1}, 1 \leq j \leq N_e\}$, for the $i$th local filter representing $p(\boldsymbol{x}_{i,k}|\mathbb{Y}_{i,k-1})$, can be expressed as

$$\hat{\boldsymbol{x}}^{(j)}_{i,k|k-1} = \boldsymbol{f}_i\left(\hat{\boldsymbol{x}}^{(j)}_{i,k-1|k-1}, \boldsymbol{u}^{(j)}_{k-1}\right) + \boldsymbol{v}^{(j)}_{i,k} \ .$$

The sample mean and covariance of the above ensemble are computed as

$$\hat{\boldsymbol{x}}_{i,k|k-1} = \frac{1}{N_e}\sum_{j=1}^{N_e} \hat{\boldsymbol{x}}^{(j)}_{i,k|k-1} \ ,$$

$$\boldsymbol{P}_{i,k|k-1} = \frac{1}{N_e - 1}\boldsymbol{E}^x_{i,k|k-1}\left(\boldsymbol{E}^x_{i,k|k-1}\right)^T \ ,$$

being $\boldsymbol{E}^x_{i,k|k-1} = [(\hat{\boldsymbol{x}}^{(1)}_{i,k|k-1} - \hat{\boldsymbol{x}}_{i,k|k-1}), \ldots, (\hat{\boldsymbol{x}}^{(N_e)}_{i,k|k-1} - \hat{\boldsymbol{x}}_{i,k|k-1})]$. Analogously, an ensemble of samples $\{\hat{\boldsymbol{y}}^{(j)}_{i,k|k-1}, 1 \leq j \leq N_e\}$, which represents $p(\boldsymbol{y}_{i,k}|\mathbb{Y}_{i,k-1})$, can be expressed as

$$\hat{\boldsymbol{y}}^{(j)}_{i,k|k-1} = \boldsymbol{h}_i\left(\hat{\boldsymbol{x}}^{(j)}_{i,k|k-1}, \boldsymbol{u}^{(j)}_{k}\right) + \boldsymbol{n}^{(j)}_{i,k} \ ,$$

where $\{\boldsymbol{n}^{(j)}_{i,k}, 1 \leq j \leq N_e\}$ is generated using the Gaussian distribution $\mathcal{N}(\boldsymbol{0}, \boldsymbol{R}_{i,k})$ to represent the measurement noise. The sample mean and covariance of the above ensemble are computed as

$$\hat{\boldsymbol{y}}_{i,k|k-1} = \frac{1}{N_e}\sum_{j=1}^{N_e} \hat{\boldsymbol{y}}^{(j)}_{i,k|k-1} \ ,$$

$$\boldsymbol{P}^y_{i,k|k-1} = \frac{1}{N_e - 1}\boldsymbol{E}^y_{i,k|k-1}\left(\boldsymbol{E}^y_{i,k|k-1}\right)^T \ ,$$

being $\boldsymbol{E}^y_{i,k|k-1} = [(\hat{\boldsymbol{y}}^{(1)}_{i,k|k-1} - \hat{\boldsymbol{y}}_{i,k|k-1}), \ldots, (\hat{\boldsymbol{y}}^{(N_e)}_{i,k|k-1} - \hat{\boldsymbol{y}}_{i,k|k-1})]$. Further, the cross-covariance between $\boldsymbol{x}_{i,k}$ and $\boldsymbol{y}_{i,k}$ given $\mathbb{Y}_{i,k-1}$ can be defined as

$$\boldsymbol{P}^{xy}_{i,k|k-1} = \frac{1}{N_e - 1}\boldsymbol{E}^x_{i,k|k-1}\left(\boldsymbol{E}^y_{i,k|k-1}\right)^T \ .$$

Using the latest measurement $\boldsymbol{y}_{i,k}$, each member $(\hat{\boldsymbol{x}}^{(j)}_{i,k|k-1})$ of the *a priori* ensemble can be updated according to the (13) and (14). The *a posteriori* ensemble $\{\hat{\boldsymbol{x}}^{(j)}_{i,k|k}, 1 \leq j \leq N_e\}$ can be considered an approximate representation of $p(\boldsymbol{x}_{i,k}|\mathbb{Y}_{i,k})$, thus the updated estimate of the mean and covariance can be computed as

$$\hat{\boldsymbol{x}}_{i,k|k} = \frac{1}{N_e}\sum_{j=1}^{N_e} \hat{\boldsymbol{x}}^{(j)}_{i,k|k} \ , \quad \boldsymbol{P}_{i,k|k} = \frac{1}{N_e - 1}\boldsymbol{E}^x_{i,k|k}\left(\boldsymbol{E}^x_{i,k|k}\right)^T,$$

where the matrix $\boldsymbol{E}^x_{i,k|k}$ is defined as $\boldsymbol{E}^x_{i,k|k} = [(\hat{\boldsymbol{x}}^{(1)}_{i,k|k} - \hat{\boldsymbol{x}}_{i,k|k}), \ldots, (\hat{\boldsymbol{x}}^{(N_e)}_{i,k|k} - \hat{\boldsymbol{x}}_{i,k|k})]$. The ensemble-based prediction and update are recursively repeated. The time update and the measurement update of the EnKF are summarized as follows.

*Time Update:*

$$\hat{\boldsymbol{x}}^{(j)}_{i,k|k-1} = \boldsymbol{f}_i\left(\hat{\boldsymbol{x}}^{(j)}_{i,k-1|k-1}, \boldsymbol{u}^{(j)}_{k-1}\right) + \boldsymbol{v}^{(j)}_{i,k} \ ,$$

$$\hat{\boldsymbol{y}}^{(j)}_{i,k|k-1} = \boldsymbol{h}_i\left(\boldsymbol{x}^{(j)}_{i,k|k-1}, \boldsymbol{u}^{(j)}_{k}\right) + \boldsymbol{n}^{(j)}_{i,k} \ ,$$

$$\hat{\boldsymbol{x}}_{i,k|k-1} = \frac{1}{N_e}\sum_{j=1}^{N_e} \hat{\boldsymbol{x}}^{(j)}_{i,k|k-1} \ ,$$

$$\hat{\boldsymbol{y}}_{i,k|k-1} = \frac{1}{N_e}\sum_{j=1}^{N_e} \hat{\boldsymbol{y}}^{(j)}_{i,k|k-1} \ ,$$

$$\boldsymbol{E}^x_{i,k|k-1} = \left[(\hat{\boldsymbol{x}}^{(1)}_{i,k|k-1} - \hat{\boldsymbol{x}}_{i,k|k-1}), \ldots, (\hat{\boldsymbol{x}}^{(N_e)}_{i,k|k-1} - \hat{\boldsymbol{x}}_{i,k|k-1})\right],$$

$$\boldsymbol{E}^y_{i,k|k-1} = \left[(\hat{\boldsymbol{y}}^{(1)}_{i,k|k-1} - \hat{\boldsymbol{y}}_{i,k|k-1}), \ldots, (\hat{\boldsymbol{y}}^{(N_e)}_{i,k|k-1} - \hat{\boldsymbol{y}}_{i,k|k-1})\right],$$

$$\boldsymbol{P}_{i,k|k-1} = \frac{1}{N_e - 1}\boldsymbol{E}^x_{i,k|k-1}\left(\boldsymbol{E}^x_{i,k|k-1}\right)^T \ .$$

*Measurement Update:*

$$\boldsymbol{P}^{xy}_{i,k|k-1} = \frac{1}{N_e - 1}\boldsymbol{E}^x_{i,k|k-1}\left(\boldsymbol{E}^y_{i,k|k-1}\right)^T \ ,$$

$$\boldsymbol{P}^{y}_{i,k|k-1} = \frac{1}{N_e - 1}\boldsymbol{E}^y_{i,k|k-1}\left(\boldsymbol{E}^y_{i,k|k-1}\right)^T \ ,$$

$$\boldsymbol{K}_{i,k} = \boldsymbol{P}^{xy}_{i,k|k-1}(\boldsymbol{P}^{y}_{i,k|k-1})^{-1} \ ,$$

$$\hat{\boldsymbol{x}}^{(j)}_{i,k|k} = \hat{\boldsymbol{x}}^{(j)}_{i,k|k-1} + \boldsymbol{K}_{i,k}\left(\boldsymbol{y}_{i,k} - \hat{\boldsymbol{y}}^{(j)}_{i,k|k-1}\right) \ ,$$

$$\hat{\boldsymbol{x}}_{i,k|k} = \frac{1}{N_e}\sum_{j=1}^{N_e} \hat{\boldsymbol{x}}^{(j)}_{i,k|k} \ ,$$

$$\boldsymbol{E}^x_{i,k|k} = \left[(\hat{\boldsymbol{x}}^{(1)}_{i,k|k} - \hat{\boldsymbol{x}}_{i,k|k}), \ldots, (\hat{\boldsymbol{x}}^{(N_e)}_{i,k|k} - \hat{\boldsymbol{x}}_{i,k|k})\right] \ ,$$

$$\boldsymbol{P}_{i,k|k} = \frac{1}{N_e - 1}\boldsymbol{E}^x_{i,k|k}\left(\boldsymbol{E}^x_{i,k|k}\right)^T \ .$$

*3) Unscented Kalman Filter:* The UKF is a nonlinear filtering technique based on unscented transform, where the first-order linearization using Jacobian matrices is replaced with a deterministic sampling method that accurately captures the

posterior mean and covariance of the distribution using a set of weighted sample points, namely *sigma points*.

Referring to the state vector as defined in (12), the set of sigma points $\boldsymbol{\chi}_{i,k-1|k-1}$ for $\boldsymbol{x}_{i,k-1}$ can be generated as

$$\boldsymbol{\chi}_{i,j,k-1|k-1} = \begin{cases} \hat{\boldsymbol{x}}_{i,k-1|k-1}, & j=0 \\ \hat{\boldsymbol{x}}_{i,k-1|k-1} + \sqrt{n_x+\lambda}\left(\boldsymbol{P}^{1/2}_{i,k-1|k-1}\right)_j, & j=1,\ldots,n_x \\ \hat{\boldsymbol{x}}_{i,k-1|k-1} - \sqrt{n_x+\lambda}\left(\boldsymbol{P}^{1/2}_{i,k-1|k-1}\right)_{j-n_x}, & j=n_x,\ldots,2n_x \end{cases}$$

where $\hat{\boldsymbol{x}}_{i,k-1|k-1}$ and $\boldsymbol{P}_{i,k-1|k-1}$ are the mean and covariance of $\boldsymbol{x}_{i,k-1}$. The scaling parameter $\lambda$ is selected according to [40]. The sigma points are propagated through the nonlinear function $\boldsymbol{f}_i(\cdot,\cdot)$ to generate $\boldsymbol{\chi}_{i,j,k|k-1} = \boldsymbol{f}_i(\boldsymbol{\chi}_{i,j,k-1|k-1}, \boldsymbol{u}_{k-1})$ and used to compute the *a priori* state estimate and covariance as follows

$$\hat{\boldsymbol{x}}_{i,k|k-1} = \sum_{j=0}^{2n_x} W_j^{(m)} \boldsymbol{\chi}_{i,j,k|k-1}, \tag{15}$$

$$\boldsymbol{P}_{i,k|k-1} = \sum_{j=0}^{2n_x} W_j^{(c)} \left(\boldsymbol{\chi}_{i,j,k|k-1} - \hat{\boldsymbol{x}}_{i,k|k-1}\right) \left(\boldsymbol{\chi}_{i,j,k|k-1} - \hat{\boldsymbol{x}}_{i,k|k-1}\right)^T + \boldsymbol{Q}_{i,k}, \tag{16}$$

where the weights $W_j^{(m)}$ and $W_j^{(c)}$ for the $j$th sigma point correspond to the mean and covariance, and are defined as

$$W_0^{(m)} = \frac{\lambda}{\lambda+n_x}, \quad W_0^{(c)} = \frac{\lambda}{\lambda+n_x} + (1-\alpha^2+\beta),$$
$$W_j^{(c)} = W_j^{(m)} = \frac{1}{2(\lambda+n_x)}, \quad j=1,\ldots,2n_x, \tag{17}$$

where the parameter $\beta$ in (17) is used to incorporate the prior information of the distribution of $\boldsymbol{x}$. For the update step, the sigma points $\boldsymbol{\chi}_{i,j,k|k-1}$ are transformed as $\boldsymbol{\gamma}_{i,j,k|k-1} = \boldsymbol{h}_i(\boldsymbol{\chi}_{i,j,k|k-1}, \boldsymbol{u}_k)$. The predicted mean and covariance of $\boldsymbol{y}_{i,k}$ and the cross-covariance between $\boldsymbol{x}_{i,k}$ and $\boldsymbol{y}_{i,k}$ are computed as

$$\hat{\boldsymbol{y}}_{i,k|k-1} = \sum_{j=0}^{2n_x} W_j^{(m)} \boldsymbol{\gamma}_{i,j,k|k-1},$$

$$\boldsymbol{P}^y_{i,k|k-1} = \sum_{j=0}^{2n_x} W_j^{(c)} \left(\boldsymbol{\gamma}_{i,j,k|k-1} - \hat{\boldsymbol{y}}_{i,k|k-1}\right) \left(\boldsymbol{\gamma}_{i,j,k|k-1} - \hat{\boldsymbol{y}}_{i,k|k-1}\right)^T + \boldsymbol{R}_{i,k},$$

$$\boldsymbol{P}^{xy}_{i,k|k-1} = \sum_{j=0}^{2n_x} W_j^{(c)} \left(\boldsymbol{\chi}_{i,j,k|k-1} - \hat{\boldsymbol{x}}_{i,k|k-1}\right) \left(\boldsymbol{\gamma}_{i,j,k|k-1} - \hat{\boldsymbol{y}}_{i,k|k-1}\right)^T.$$

The *a posteriori* state estimate is evaluated according to (13) and (14), while the covariance as

$$\boldsymbol{P}_{i,k|k} = \boldsymbol{P}_{i,k|k-1} - \boldsymbol{K}_{i,k} \boldsymbol{P}^y_{i,k|k-1} \boldsymbol{K}^T_{i,k}. \tag{18}$$

The above equations are summarized as time and measurement updates below.

*Time Update:*

$$\boldsymbol{\chi}_{i,j,k|k-1} = \boldsymbol{f}_i(\boldsymbol{\chi}_{i,j,k-1|k-1}, \boldsymbol{u}_{k-1}),$$

$$\hat{\boldsymbol{x}}_{i,k|k-1} = \sum_{j=0}^{2n_x} W_j^{(m)} \boldsymbol{\chi}_{i,j,k|k-1},$$

$$W_0^{(m)} = \frac{\lambda}{\lambda+n_x}, \quad W_0^{(c)} = \frac{\lambda}{\lambda+n_x} + (1-\alpha^2+\beta),$$
$$W_j^{(c)} = W_j^{(m)} = \frac{1}{2(\lambda+n_x)}, \quad j=1,\ldots,2n_x,$$

$$\boldsymbol{\gamma}_{i,j,k|k-1} = \boldsymbol{h}_i(\boldsymbol{\chi}_{i,j,k|k-1}, \boldsymbol{u}_k),$$

$$\hat{\boldsymbol{y}}_{i,k|k-1} = \sum_{j=0}^{2n_x} W_j^{(m)} \boldsymbol{\gamma}_{i,j,k|k-1},$$

$$\boldsymbol{P}_{i,k|k-1} = \sum_{j=0}^{2n_x} W_j^{(c)} \left(\boldsymbol{\chi}_{i,j,k|k-1} - \hat{\boldsymbol{x}}_{i,k|k-1}\right) \left(\boldsymbol{\chi}_{i,j,k|k-1} - \hat{\boldsymbol{x}}_{i,k|k-1}\right)^T + \boldsymbol{Q}_{i,k}.$$

*Measurement Update:*

$$\boldsymbol{P}^y_{i,k|k-1} = \sum_{j=0}^{2n_x} W_j^{(c)} \left(\boldsymbol{\gamma}_{i,j,k|k-1} - \hat{\boldsymbol{y}}_{i,k|k-1}\right) \left(\boldsymbol{\gamma}_{i,j,k|k-1} - \hat{\boldsymbol{y}}_{i,k|k-1}\right)^T + \boldsymbol{R}_{i,k},$$

$$\boldsymbol{P}^{xy}_{i,k|k-1} = \sum_{j=0}^{2n_x} W_j^{(c)} \left(\boldsymbol{\chi}_{i,j,k|k-1} - \hat{\boldsymbol{x}}_{i,k|k-1}\right) \left(\boldsymbol{\chi}_{i,j,k|k-1} - \hat{\boldsymbol{y}}_{i,k|k-1}\right)^T,$$

$$\boldsymbol{K}_{i,k} = \boldsymbol{P}^{xy}_{i,k|k-1} (\boldsymbol{P}^y_{i,k|k-1})^{-1},$$

$$\hat{\boldsymbol{x}}_{i,k|k} = \hat{\boldsymbol{x}}_{i,k|k-1} + \boldsymbol{K}_{i,k}(\boldsymbol{y}_{i,k} - \hat{\boldsymbol{y}}_{i,k|k-1}),$$

$$\boldsymbol{P}_{i,k|k} = \boldsymbol{P}_{i,k|k-1} - \boldsymbol{K}_{i,k} \boldsymbol{P}^y_{i,k|k-1} \boldsymbol{K}^T_{i,k}.$$

### D. Data-Fusion for SFDIA

When sensor faults occur, faulty measurements affect multiple local filters and related estimates. The main challenge of an efficient SFDIA framework is its ability to perform detection, isolation, and accommodation while considering that the results from each task affect the remaining tasks.

For fault detection, the state-variance vector ($\boldsymbol{\xi}_k \in \mathbb{R}^{n_x \times 1}$) and the state residual ($r_{i,k}$) are employed as anomaly indicators, where the $\ell$th entry of the state-variance vector is

$$\xi_k^{(\ell)} = \frac{1}{N} \sum_{i=1}^{N} \left( \hat{x}^{(\ell)}_{i,k|k} - \frac{1}{N} \sum_{i=1}^{N} \left( \hat{x}^{(\ell)}_{i,k|k} \right) \right)^2, \tag{19}$$

being $\hat{x}^{(\ell)}_{i,k|k}$ the $\ell$th entry of state vector estimate, and the residual $r_{i,k}$ of the $i$th local filter is defined as

$$r_{i,k} = \left[ (\hat{\boldsymbol{x}}_{i,k|k} - \hat{\boldsymbol{x}}_{m,k})^T (\hat{\boldsymbol{x}}_{i,k|k} - \hat{\boldsymbol{x}}_{m,k}) \right]^{\frac{1}{2}}. \tag{20}$$

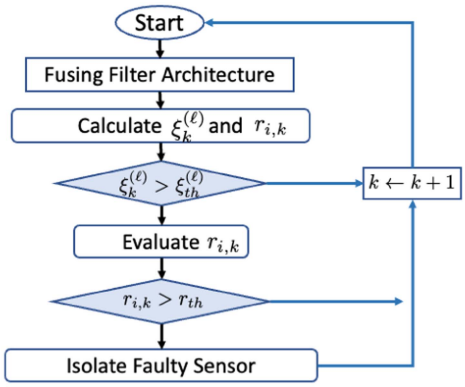


Fig. 3. KF-based data-fusion architecture.

TABLE II
PARAMETERS UTILIZED FOR SIMULATIONS

| Parameters | Values |
|---|---|
| $L$ | 150 km |
| $d$ | 1.4 m |
| $\epsilon$ | 0.016 mm |
| $T_s$ | 5$^o$C |
| $U$ | 2.84 Wm$^{-2}$K$^{-1}$ |

A fault will make the entries of the state-variance vector and the residuals high, thus facilitating detection. However, the interaction among the various components of the architecture coupled with the system's non-linearity makes the isolation not trivial. Hence, proper design of local filters and related grouping of measurements is crucial for isolation capability: for a system equipped with $N$ sensors, we consider $N$ local filters, each receiving $N-1$ sensor measurements as input (each one with a different sensor excluded).

More specifically, we use the state-variance vector ($\boldsymbol{\xi}_k$) for detection, comparing its entries with a predefined threshold condition, and the residual ($r_{i,k}$) for isolation, identifying the one exhibiting the largest value. For example, if the $j$th sensor is faulty, then the $N-1$ local filters processing the $j$th sensor measurement are affected and the single local filter devoid of the $j$th sensor measurement is not. This reflects in the information mixture which is computed using $N-1$ inaccurate estimates and 1 accurate estimate, resulting in the global state estimate ($\hat{\boldsymbol{x}}_{m,k}$) being inaccurate as well, while the residual associated to the accurate local filter ($r_{j,k}$) being larger than the other residuals. The flowchart of the mechanism exploiting data fusion and the computation of the state-variance vector and the residuals to perform detection and isolation is illustrated in Fig. 3.

## IV. DATA GENERATION

### A. Fault-Free Data

The simulated data for a transient flow in the natural-gas pipeline is generated using a numerical solution of the flow model discussed in Section II. We choose a high-pressure natural-gas pipeline with the parameters listed in Table II.

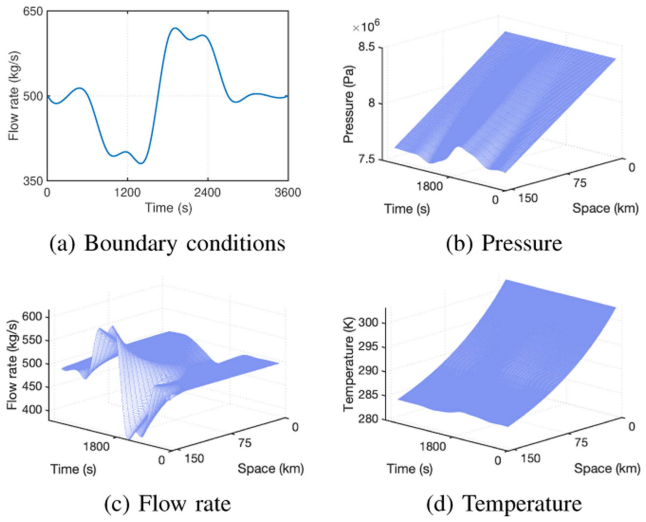


(a) Boundary conditions (b) Pressure

(c) Flow rate (d) Temperature

Fig. 4. Simulated data.

The simulations are done for $t_f \in [0, 3600\text{ s}]$ with $p(0,t) = 8.4$ MPa, $T(0,t) = 303.15$ K and $\dot{m}(L,t) = f(t)$. The boundary conditions are selected similar to those in [8]. In the numerical solution of the transient-flow model, the following spatial and temporal step sizes are considered: $\Delta s = 7500\,\text{m}$ and $\Delta t = 10\,\text{s}$. Fig. 4 displays the boundary conditions and related spatial-temporal evolution of the state variables devoid of additive model noise.

Zero-mean white Gaussian noise ($q_j[k]$) is added to the generated ideal (without noise and without faults) value ($x_j[k]$), i.e. (referring to the $k$th sample from the $j$th sensor)

$$y_j[k] = x_j[k] + q_j[k], \tag{21}$$

where $y_j[k]$ is the noisy fault-free measurement.

### B. Faulty Data

In order to evaluate the SFDIA performance, synthetic fault signals have been generated and superimposed to the simulated data from the transient-flow model, thus mimicking sensor measurements in the presence of sensor failures. Faults in sensors could be of various types with bias, drift, freezing, and random faults being among the most popular [12], [13]. Without compromising generality, we considered bias and drift faults to represent hard and soft failures, respectively. The mathematical models for these types of faults are:

*Bias fault:* A constant level (or bias) $b$ is added for $M$ consecutive samples to the sensor measurements, i.e.

$$y_j^f[k] = \begin{cases} y_j[k] + b, & 0 \le k - m \le M \\ y_j[k], & \text{else} \end{cases},$$

where $y_j^f[k]$ is the faulty measurement, and $m$ is the starting time of the fault.

TABLE III
MEASUREMENT NOISE FOR PRESSURE, TEMPERATURE AND FLOW RATE CORRESPONDING TO DIFFERENT SNR CASES

| Measurement noise | Pressure | Flow rate | Temperature |
|---|---|---|---|
| High SNR | $\mathcal{N}(0, 0.00005^2)$ | $\mathcal{N}(0, 0.25^2)$ | $\mathcal{N}(0, 0.15^2)$ |
| Moderate SNR | $\mathcal{N}(0, 0.0005^2)$ | $\mathcal{N}(0, 2.5^2)$ | $\mathcal{N}(0, 1.5^2)$, |
| Low SNR | $\mathcal{N}(0, 0.001^2)$ | $\mathcal{N}(0, 10^2)$ | $\mathcal{N}(0, 6^2)$ |

*Drift fault:* The actual measurement drifts up (with a maximum bias level $b$) within $M$ time instants, i.e.

$$y_j^f[k] = \begin{cases} y_j[k] + \frac{b(k-m+1)}{M}, & 0 \le k-m \le M \\ y_j[k] + b, & M \le k-m \le M+K \\ y_j[k], & \text{else} \end{cases},$$

where $K$ represents the number of samples during which the drift fault maintains the saturated bias level $b$. Additionally, we stressed the impact of the drift by assuming $M > K$.

## V. NUMERICAL RESULTS

To illustrate the performance of the proposed technique for the transient-flow model, we considered scenarios with and without sensor faults. For non-faulty scenarios, we only consider noise in the measurements to evaluate the state estimation performance of the architecture. The effectiveness of the data-fusion SFDIA architecture is then validated in faulty scenarios.

### A. Non-Faulty Scenarios

We compare the performance of the fusing EKF, fusing EnKF, and fusing UKF with their corresponding basic counterparts against the measurement noise. To validate the robustness of the proposed architecture, we have considered three different signal-to-noise ratios (SNRs), i.e., low, moderate, and high. The distribution of the measurement noise for all three cases is demonstrated in Table III.

For EnKF, the size of the ensemble $N_e$ is chosen as 40. In case of UKF, the scaling parameters $\alpha$ and $\beta$ are set to $10^{-3}$ and 2, respectively [40]. The *a priori* estimate of the error covariance matrix $\boldsymbol{P}_{i,0|0}$ is considered as an identity matrix. The standard deviation of the process noise is considered 10% lower than that of the measurement noise. The $\boldsymbol{Q}_{i,k}$ and $\boldsymbol{R}_{i,k}$ matrices are also diagonal matrices with diagonal entries corresponding to the process and measurement noise variances, respectively.

For the data-fusion architecture, $N = 63$ local filters are considered, where each local filter has 62 sensor measurements. The estimation performance of different methods is assessed in terms of spatial and temporal root mean square error (RMSE), which is averaged over $\tau$ iterations with different random seeds in each iteration. The evaluation metric RMSE is defined as

$$\text{RMSE} = \frac{1}{\tau}\sum_{i=1}^{\tau}\left(\frac{\|\boldsymbol{X} - \hat{\boldsymbol{X}}\|_F}{\sqrt{N_s N_k}}\right),$$

where $\|\cdot\|_F$ is the Frobenius norm, the true state matrix $\boldsymbol{X}$ and the estimated state matrix $\hat{\boldsymbol{X}}$ are defined as $\boldsymbol{X} = [\boldsymbol{x}_{i,1|1}, \boldsymbol{x}_{i,2|2}, \ldots, \boldsymbol{x}_{i,N_k|N_k}]$ and $\hat{\boldsymbol{X}} = [\hat{\boldsymbol{x}}_{i,1|1}, \hat{\boldsymbol{x}}_{i,2|2}, \ldots, \hat{\boldsymbol{x}}_{i,N_k|N_k}]$, respectively. Further, the number of spatial nodes $N_s$ and the number of time steps $N_k$ are defined as $N_s = L/\Delta s$ and $N_k = t_f/\Delta t$, respectively, and $\tau = 10$. The estimation performance in terms of the RMSE for fusing EnKF, fusing UKF, and fusing EKF along with the corresponding basic filters is explicitly summarized in Table IV: fusing filters have higher estimation accuracy in comparison to the basic counterparts with the fusing EnKF and fusing UKF being preferable in overall performance.

TABLE IV
COMPARISON OF RMSE FOR DIFFERENT FILTERS UNDER NON-FAULTY SCENARIOS

| SNR | Filter | Pressure ($10^{-3}$MPa) | Flow rate (kg/s) | Temperature (K) |
|---|---|---|---|---|
| High | Fusing EnKF | 0.13547 | 0.7441 | 0.3500 |
| | Fusing UKF | 0.082194 | 0.4172 | 0.2120 |
| | Fusing EKF | 1.0727 | 0.5445 | 0.1009 |
| | EnKF | 0.3829 | 1.2886 | 0.6622 |
| | UKF | 0.070686 | 0.1689 | 0.2329 |
| | EKF | 1.4684 | 0.7488 | 0.2009 |
| Moderate | Fusing EnKF | 0.219 | 1.0672 | 0.5879 |
| | Fusing UKF | 0.12307 | 0.6463 | 0.3472 |
| | Fusing EKF | 3.4249 | 0.8852 | 0.3427 |
| | EnKF | 0.44852 | 0.8669 | 0.3051 |
| | UKF | 0.15820 | 0.8022 | 0.4490 |
| | EKF | 2.6018 | 0.8695 | 0.3328 |
| Low | Fusing EnKF | 0.4031 | 2.3451 | 1.4395 |
| | Fusing UKF | 0.33872 | 1.9596 | 1.0892 |
| | Fusing EKF | 0.93483 | 0.6716 | 0.1176 |
| | EnKF | 0.43635 | 1.8683 | 1.8683 |
| | UKF | 0.449303 | 2.6353 | 1.5484 |
| | EKF | 7.1529 | 2.0372 | 1.1611 |

### B. Faulty Scenarios

The effectiveness of the proposed schemes is investigated in the presence of various types of sensor faults. More specifically, we consider weak and strong faults represented by bias and drift, respectively. To represent weak (resp. strong) faults, the absolute level $b$ is assumed to be uniformly distributed between 20% and 40% (resp. 60% and 90%) of the data amplitude. Also, a random sign is considered for the actual level, so that both positive and negative faults are randomly generated. The fault lengths ($M$ and $K$) are also assumed to be uniformly distributed between 10 and 20 consecutive samples. It should be noted that choosing a uniform distribution of fault level $b$ and fault lengths makes it easier to evaluate the performance of the SFDIA without focusing on a particular fault level or length. Moreover, to evaluate the robustness of the fusing architecture against consecutive faults, we choose random faulty sensors among the available spatial measurements generated by PDEs. For this scenario, we consider measurement noise corresponding to the moderate SNR.

Numerical results have been obtained via Monte Carlo simulations with 50 runs using MATLAB software. The probabilities of detection and false alarm, computed on a sample-by-sample basis, are selected as metrics to evaluate the detection performance of the data-fusion SFDIA architecture. More specifically, Fig. 5 shows the receiver operating characteristic (ROC) curves for

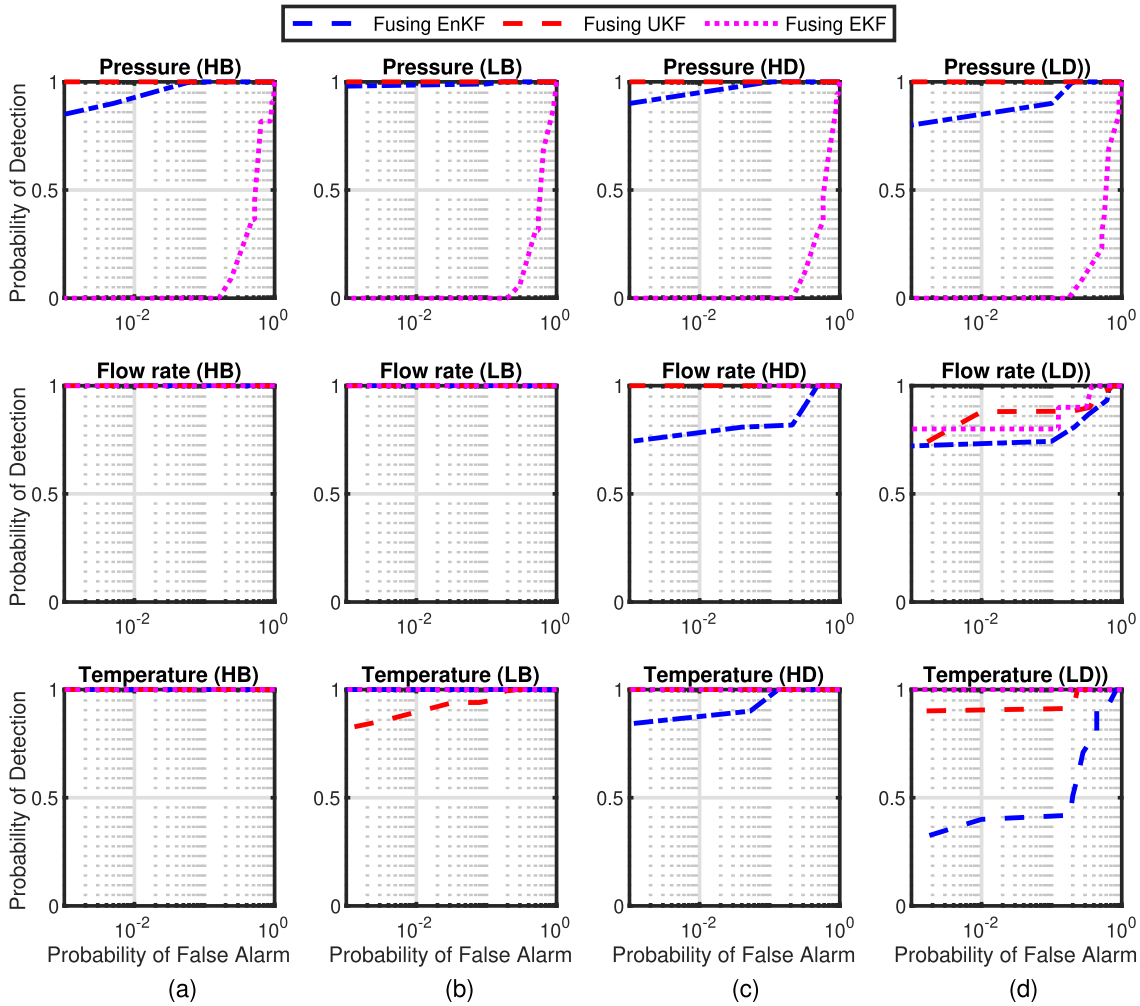


Fig. 5. ROC plots comparing detection performance of fusing filters for different fault types: (a) strong bias (SB), (b) weak bias (WB), (c) strong drift (SD), and (d) weak drift (WD).

each physical quantity (i.e. pressure, flow rate, and temperature) by varying their respective threshold value defined in (19). The results demonstrate that the proposed SFDIA architecture can detect sensor faults effectively even in the case of weak faults. Again, fusing UKF and fusing EnF are confirmed a better choice with respect to fusing EKF, mainly due to their capability to better handle high non-linearity, which are significant in the gas flow model (especially related to the pressure).

Further, the isolation matrix is chosen as a performance metric to demonstrate the isolation capability of the proposed SFDIA architecture. Fig. 6 illustrates the confusion matrices explicitly for the fusing EnKF, fusing UKF, and fusing EKF to demonstrate their efficacy in isolating the weak bias faults. The fusing EnKF demonstrates the capability to accurately predict and isolate all faulty sensors with only a few false alarms. In contrast, the fusing UKF accurately predicts faults related to the pressure and flow rate sensors while producing a small number of false alarms. However, it does not provide precise predictions for faults in the temperature sensors. Additionally, the fusing EKF accurately predicts faults in the temperature sensors but does not make any predictions corresponding to the pressure sensor faults. Further, the performance of the proposed SFDIA is computed in terms of detection accuracy and RMSE for a fixed threshold. The detection accuracy of fusing EnKF, fusing UKF, and fusing EKF for different faults under different SNR scenarios, i.e., low, medium, and high SNR, is presented in Tables V, VI, and VII, respectively. It can be distinctly observed from the results that all three variants exhibit high detection performance under moderate and high SNR scenarios. Additionally, we compare the RMSE performance of the fusing architectures with and without FDI in Fig. 7, considering moderate SNR. The outcomes emphasize that the fusing architectures with FDI yield lower RMSE values compared to those without FDI. Meanwhile, the fused EKF demonstrates notably higher RMSE values, especially evident in scenarios without FDI. This discrepancy arises from its difficulty in accurately handling the nonlinear system, leading to significant deviations when confronted with faulty measurements. Furthermore, the fusing architectures incorporating FDI exhibit superior performance compared to their counterparts without FDI.

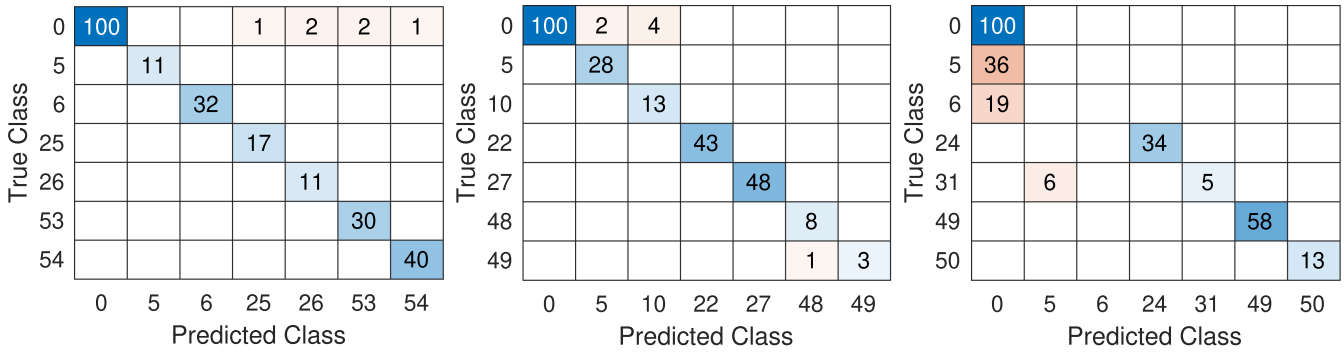


Fig. 6. Confusion matrix for weak bias faults (a) fusing EnKF (b) fusing UKF (c) fusing EKF. Here the index 0 indicates the non-faulty case.

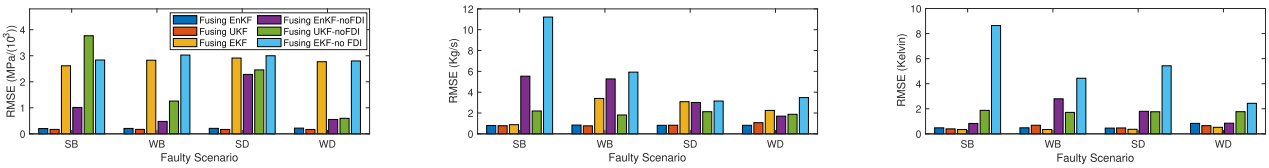


Fig. 7. Comparing RMSE of three fusing filters when four different faults, including strong bias (SB), weak bias (WB), strong drift (SD), and weak drift (WD), are added to (a) pressure (b) flow rate (c) temperature sensors.

TABLE V
LOW SNR SCENARIO: CONTRASTING THE ACCURACY OF THREE FUSING FILTERS WHEN FOUR DIFFERENT FAULTS, NAMELY STRONG BIAS (SB), WEAK BIAS (WB), STRONG DRIFT (SD), AND WEAK DRIFT (WD), ARE ADDED TO THE PRESSURE, FLOW RATE, AND TEMPERATURE SENSORS

| Fault | Filter | Bias(%) | | Drift(%) | |
|---|---|---|---|---|---|
| | | Strong | Weak | Strong | Weak |
| Pressure | Fusing EnKF | 86.11 | 86.11 | 83.33 | 72.22 |
| | Fusing UKF | **100** | **97.22** | **100** | **100** |
| | Fusing EKF | 45.00 | 41.67 | 46.67 | 41.67 |
| Flow rate | Fusing EnKF | 77.78 | 72.22 | 88.89 | **86.11** |
| | Fusing UKF | **100** | **100** | 86.11 | 63.89 |
| | Fusing EKF | 88.33 | 95 | **91.67** | 83.33 |
| Temperature | Fusing EnKF | 86.11 | 86.11 | 83.33 | 77.78 |
| | Fusing UKF | **100** | **100** | **88.89** | **86.11** |
| | Fusing EKF | **100** | **100** | 83.33 | 76.67 |

TABLE VI
MODERATE SNR SCENARIO: CONTRASTING THE ACCURACY OF THREE FUSING FILTERS WHEN FOUR DIFFERENT FAULTS, NAMELY STRONG BIAS (SB), WEAK BIAS (WB), STRONG DRIFT (SD), AND WEAK DRIFT (WD), ARE ADDED TO THE PRESSURE, FLOW RATE, AND TEMPERATURE SENSORS

| Fault | Filter | Bias(%) | | Drift(%) | |
|---|---|---|---|---|---|
| | | Strong | Weak | Strong | Weak |
| Pressure | Fusing EnKF | 89.44 | 88.89 | 87.78 | 87.50 |
| | Fusing UKF | **100** | **100** | **100** | **100** |
| | Fusing EKF | 46.67 | 45.00 | 61.67 | 58.89 |
| Flow rate | Fusing EnKF | 88.61 | 83.89 | 79.72 | 67.78 |
| | Fusing UKF | **100** | **100** | **94.17** | 83.89 |
| | Fusing EKF | 100 | 97.78 | 90.28 | **92.22** |
| Temperature | Fusing EnKF | 91.76 | 88.25 | 81.11 | 62.78 |
| | Fusing UKF | 97.22 | 97.92 | 94.44 | 90.83 |
| | Fusing EKF | **100** | **100** | **97.50** | **93.61** |

TABLE VII
HIGH SNR SCENARIO: CONTRASTING THE ACCURACY OF THREE FUSING FILTERS WHEN FOUR DIFFERENT FAULTS, NAMELY STRONG BIAS (SB), WEAK BIAS (WB), STRONG DRIFT (SD), AND WEAK DRIFT (WD), ARE ADDED TO THE PRESSURE, FLOW RATE, AND TEMPERATURE SENSORS

| Fault | Filter | Bias(%) | | Drift(%) | |
|---|---|---|---|---|---|
| | | Strong | Weak | Strong | Weak |
| Pressure | Fusing EnKF | **100** | **100** | 86.11 | 80.56 |
| | Fusing UKF | **100** | 97.22 | **100** | **91.67** |
| | Fusing EKF | 69.44 | 69.44 | 69.44 | 69.44 |
| Flow rate | Fusing EnKF | **100** | **100** | **94.44** | **88.89** |
| | Fusing UKF | **100** | 97.22 | 86.11 | 66.67 |
| | Fusing EKF | **100** | 100 | 91.67 | **88.89** |
| Temperature | Fusing EnKF | 91.67 | 94.44 | **100** | **100** |
| | Fusing UKF | 97.22 | 97.22 | 91.67 | 69.44 |
| | Fusing EKF | **100** | **100** | **100** | 77 |

## VI. CONCLUSION

This paper investigated a model-based SFDIA architecture designed for natural gas pipelines undergoing transient flow conditions. The proposed distributed filtering-based architecture assists in fault identification by merging data gathered from multiple sensors. The fusing architecture consists of several local filters and an information mixer. These local filters operate concurrently in parallel to estimate state variables, which are subsequently combined in the information mixer to compute fault-free state estimates. Three different versions of the fusion filter, including the fusing UKF, fusing EKF, and fusing EnKF were specifically crafted for fault diagnosis. Validation of these methods using simulated data demonstrates the effectiveness of

the proposed framework, especially in identifying, isolating, and handling various sensor faults using diverse local filters.

Future work will focus on exploring fault diagnosis in real-world, large-scale distributed industrial processes. To enhance the accuracy of the proposed architecture, an adaptive thresholding scheme for fault detection can be developed, and other non-linear Bayesian filtering methods such as the particle filter can be integrated. Moreover, there is potential for investigating architectures capable of effectively handling scenarios involving multiple simultaneous sensor faults.

## REFERENCES


[1] T. B. Quy and J.-M. Kim, "Real-time leak detection for a gas pipeline using a k-NN classifier and hybrid AE features," *Sensors*, vol. 21, no. 2, p. 367, 2021.

[2] G. Tabella, N. Paltrinieri, V. Cozzani, and P. S. Rossi, "Wireless sensor networks for detection and localization of subsea oil leakages," *IEEE Sensors J.*, vol. 21, no. 9, pp. 10890–10904, May 2021.

[3] L. Hou, D. Wang, B. Du, X. Qian, and M. Yuan, "Gas concentration detection via multi-channeled air sampling method," *Sensor Rev.*, vol. 37, no. 2, pp. 187–195, 2017.

[4] Q. Tan et al., "A new sensor fault diagnosis method for gas leakage monitoring based on the naive bayes and probabilistic neural network classifier," *Measurement*, vol. 194, 2022, Art. no. 111037.

[5] C. Verde, "Multi-leak detection and isolation in fluid pipelines," *Control Eng. Pract.*, vol. 9, no. 6, pp. 673–682, 2001.

[6] R. Doshmanziari, H. Khaloozadeh, and A. Nikoofard, "Gas pipeline leakage detection based on sensor fusion under model-based fault detection framework," *J. Petroleum Sci. Eng.*, vol. 184, 2020, Art. no. 106581.

[7] J. Delgado-Aguiñaga, G. Besancon, O. Begovich, and J. Carvajal, "Multi-leak diagnosis in pipelines based on extended Kalman filter," *Control Eng. Pract.*, vol. 49, pp. 139–148, 2016.

[8] F. Uilhoorn, "Comparison of Bayesian estimation methods for modeling flow transients in gas pipelines," *J. Natural Gas Sci. Eng.*, vol. 38, pp. 159–170, 2017.

[9] M. M. Syed, T. A. Lemma, S. K. Vandrangi, and T. N. Ofei, "Recent developments in model-based fault detection and diagnostics of gas pipelines under transient conditions," *J. Natural Gas Sci. Eng.*, vol. 83, 2020, Art. no. 103550.

[10] A. Rasheed, O. San, and T. Kvamsdal, "Digital twin: Values, challenges and enablers from a modeling perspective," *IEEE Access*, vol. 8, pp. 21980–22012, 2020.

[11] Z. Zhang et al., "Optimization monitoring distribution method for gas pipeline leakage detection in underground spaces," *Tunnelling Underground Space Technol.*, vol. 104, 2020, Art. no. 103545.

[12] H. Darvishi, D. Ciuonzo, E. R. Eide, and P. S. Rossi, "Sensor-fault detection, isolation and accommodation for digital twins via modular data-driven architecture," *IEEE Sensors J.*, vol. 21, no. 4, pp. 4827–4838, Feb. 2021.

[13] H. Darvishi, D. Ciuonzo, and P. S. Rossi, "A machine-learning architecture for sensor fault detection, isolation and accommodation in digital twins," *IEEE Sensors J.*, vol. 23, no. 3, pp. 2522–2538, Feb. 2023.

[14] W. Junru, W. Tao, and W. Junzheng, "Hybrid modelling for leak detection of long-distance gas transport pipeline," *Insight-Non-Destructive Testing Condition Monit.*, vol. 55, no. 7, pp. 372–381, 2013.

[15] S. Shao, R. Yan, Y. Lu, P. Wang, and R. X. Gao, "DCNN-based multi-signal induction motor fault diagnosis," *IEEE Trans. Instrum. Meas.*, vol. 69, no. 6, pp. 2658–2669, Jun. 2020.

[16] L. Yan, H. Zhang, X. Dong, Q. Zhou, H. Chen, and C. Tan, "Unscented Kalman-filter-based simultaneous diagnostic scheme for gas-turbine gas path and sensor faults," *Meas. Sci. Technol.*, vol. 32, no. 9, 2021, Art. no. 095905.

[17] D. Mori, H. Sugiura, and Y. Hattori, "Adaptive sensor fault detection and isolation using unscented Kalman filter for vehicle positioning," in *Proc. IEEE Intell. Transp. Syst. Conf.*, 2019, pp. 1298–1304.

[18] B. Du, Z. Shi, J. Song, H. Wang, and L. Han, "A fault-tolerant data fusion method of MEMS redundant gyro system based on weighted distributed Kalman filtering," *Micromachines*, p. 278, vol. 10, no. 5, 2019.

[19] Y. Luo, Y. Liu, W. Yang, J. Zhou, and T. Lv, "Distributed filtering algorithm based on local outlier factor under data integrity attacks," *J. Franklin Inst.*, vol. 360, pp. 9290–9306, 2023.

[20] N. S. Nokhodberiz and J. Poshtan, "Belief consensus–based distributed particle filters for fault diagnosis of non-linear distributed systems," *Proc. Inst. Mech. Engineers, Part I: J. Syst. Control Eng.*, vol. 228, pp. 123–137, 2013.

[21] P. Jin, X. Zhou, C. Wang, J. Huang, W. Zhou, and F. Lu, "A novel distributed Kalman filtering for health state recognition of aero-engine components in networked control systems," *Nonlinear Dyn.*, vol. 111, pp. 2571–2589, 2023.

[22] A. Moradi, N. K. Venkategowda, S. P. Talebi, and S. Werner, "Privacy-preserving distributed Kalman filtering," *IEEE Trans. Signal Process.*, vol. 70, pp. 3074–3089, 2022.

[23] J. Yang, F. Zhu, X. Wang, and X. Bu, "Robust sliding-mode observer-based sensor fault estimation, actuator fault detection and isolation for uncertain nonlinear systems," *Int. J. Control Automat. Syst.*, vol. 13, no. 5, pp. 1037–1046, 2015.

[24] J. Wei, G. Dong, and Z. Chen, "Model-based fault diagnosis of lithium-ion battery using strong tracking extended Kalman filter," *Energy Procedia*, vol. 158, pp. 2500–2505, 2019.

[25] W. El Sayed, M. Abd El Geliel, and A. Lotfy, "Fault diagnosis of PMSG stator inter-turn fault using extended Kalman filter and unscented Kalman filter," *Energies*, vol. 13, no. 11, p. 2972, 2020.

[26] S. D. Gupta, "A comparative study of the particle filter and the ensemble kalman filter," *Master's thesis*, Univ. Waterloo, Waterloo, ON, Canada, 2009.

[27] L. Yan, Y. Zhang, B. Xiao, Y. Xia, and M. Fu, "Fault detection for nonlinear systems with unreliable measurements based on hierarchy cubature Kalman filter," *Can. J. Chem. Eng.*, vol. 96, no. 2, pp. 497–506, 2018.

[28] S. P. Talebi and S. Werner, "Distributed Kalman filtering and control through embedded average consensus information fusion," *IEEE Trans. Autom. Control*, vol. 64, no. 10, pp. 4396–4403, Oct. 2019.

[29] A. Okatan, C. Hajiyev, and U. Hajiyeva, "Fault detection in sensor information fusion Kalman filter," *AEU- Int. J. Electron. Commun.*, vol. 63, no. 9, pp. 762–768, 2009.

[30] M. Carminati, G. Ferrari, R. Grassetti, and M. Sampietro, "Real-time data fusion and MEMS sensors fault detection in an aircraft emergency attitude unit based on Kalman filtering," *IEEE Sensors J.*, vol. 12, no. 10, pp. 2984–2992, Oct. 2012.

[31] K. Bader, B. Lussier, and W. Schön, "A fault tolerant architecture for data fusion: A real application of Kalman filters for mobile robot localization," *Robot. Auton. Syst.*, vol. 88, pp. 11–23, 2017.

[32] H. Hamadi, B. Lussier, I. Fantoni, and C. Francis, "Data fusion fault tolerant strategy for a quadrotor UAV under sensors and software faults," *ISA Trans.*, vol. 129, pp. 520–539, 2022.

[33] M. Saied, A. R. Tabikh, C. Francis, H. Hamadi, and B. Lussier, "An informational approach for fault tolerant data fusion applied to a UAV's attitude, altitude, and position estimation," *IEEE Sensors J.*, vol. 21, no. 24, pp. 27766–27778, Dec. 2021.

[34] K. Salahshoor, M. Mosallaei, and M. Bayat, "Centralized and decentralized process and sensor fault monitoring using data fusion based on adaptive extended Kalman filter algorithm," *Measurement*, vol. 41, no. 10, pp. 1059–1076, 2008.

[35] D.-J. Xin, L.-F. Shi, and X. Yu, "Distributed Kalman filter with faulty/reliable sensors based on Wasserstein average consensus," *IEEE Trans. Circuits Syst. II: Exp. Briefs*, vol. 69, no. 4, pp. 2371–2375, Apr. 2022.

[36] A. Alanwar, H. Said, and M. Althoff, "Distributed secure state estimation using diffusion Kalman filters and reachability analysis," in *Proc. IEEE 58th Conf. Decis. Control*, 2019, pp. 4133–4139.

[37] Z. Ju, H. Zhang, and Y. Tan, "Distributed deception attack detection in platoon-based connected vehicle systems," *IEEE Trans. Veh. Technol.*, vol. 69, no. 5, pp. 4609–4620, May 2020.

[38] K. Geng and N. Chulin, "Applications of multi-height sensors data fusion and fault-tolerant Kalman filter in integrated navigation system of UAV," *Procedia Comput. Sci.*, vol. 103, pp. 231–238, 2017.

[39] F. Lu, Y. Wang, J. Huang, Y. Huang, and X. Qiu, "Fusing unscented Kalman filter for performance monitoring and fault accommodation in gas turbine," *Proc. Inst. Mech. Engineers, Part G: J. Aerosp. Eng.*, vol. 232, no. 3, pp. 556–570, 2018.

[40] A. Vafamand, B. Moshiri, and N. Vafamand, "Fusing unscented Kalman filter to detect and isolate sensor faults in DC microgrids with CPLs," *IEEE Trans. Instrum. Meas.*, vol. 71, 2022, Art. no. 3503608.

[41] C. Pérez-Zuñiga, E. Chanthery, L. Travé-Massuyès, J. Sotomayor, and C. Artigues, "Decentralized diagnosis via structural analysis and integer programming," *IFAC-PapersOnLine*, vol. 51, no. 24, pp. 168–175, 2018.

[42] C. Verde and L. Torres, *Modeling and Monitoring of Pipelines and Networks*. Berlin, Germany: Springer, 2017.
[43] C. Pérez-Zuñiga, J. Sotomayor-Moriano, E. Chanthery, L. Travé-Massuyès, and M. Soto, "Flotation process fault diagnosis via structural analysis," *IFAC-PapersOnLine*, vol. 52, no. 14, pp. 225–230, 2019.
[44] C. Pérez-Zuñiga, E. Chanthery, L. Travé-Massuyès, and J. Sotomayor, "Fault-driven structural diagnosis approach in a distributed context," *IFAC-PapersOnLine*, vol. 50, no. 1, pp. 14254–14259, 2017.
[45] E. Noursadeghi and I. A. Raptis, "Reduced-order distributed fault diagnosis for large-scale nonlinear stochastic systems," *J. Dyn. Syst. Meas. Control*, vol. 140, no. 5, 2018, Art. no. 051009.
[46] Y. Feng, Y. Wang, B.-C. Wang, and H.-X. Li, "Spatial decomposition-based fault detection framework for parabolic-distributed parameter processes," *IEEE Trans. Cybern.*, vol. 52, no. 8, pp. 7319–7327, Aug. 2022.
[47] M. W. Zemansky and K. Menger, "Heat and thermodynamics," *Amer. J. Phys.*, vol. 20, no. 4, p. 248, 1952.
[48] A. Thorley and C. Tiley, "Unsteady and transient flow of compressible fluids in pipelines–A review of theoretical and some experimental studies," *Int. J. Heat Fluid Flow*, vol. 8, no. 1, pp. 3–15, 1987.
[49] C. F. Colebrook et al., "Correspondence. turbulent flow in pipes, with particular reference to the transition region between the smooth and rough pipe laws. (includes plates)," *J. Inst. Civil Engineers*, vol. 12, no. 8, pp. 393–422, 1939.
[50] E. W. Lemmon and R. T. Jacobsen, "Viscosity and thermal conductivity equations for nitrogen, oxygen, argon, and air," *Int. J. Thermophysics*, vol. 25, pp. 21–69, 2004.
[51] W. E. Schiesser, *The Numerical Method of Lines: Integration of Partial Differential Equations*. Amsterdam, The Netherlands: Elsevier, 2012.
[52] R. Courant, "Uber die partiellen differenzengleichungen der mathematischen physik," *Mathematische Annalen*, vol. 100, no. 1, pp. 32–74, 1928.
[53] Y. Bar-Shalom and L. Campo, "The effect of the common process noise on the two-sensor fused-track covariance," *IEEE Trans. Aerosp. Electron. Syst.*, vol. AES-22, no. 6, pp. 803–805, Nov. 1986.

**Khadija Shaheen** (Member, IEEE) received the M.Sc. degree in electrical engineering with specialization in digital systems and signal processing from the School of Electrical Engineering and Computer Science, National University of Sciences and Technology, Islamabad, Pakistan. She is currently working toward the Ph.D. degree in electronics with the Department Electronic Systems, Norwegian University of Science and Technology, Trondheim, Norway. Her research interests include sensor validation, machine learning, and digital signal processing.

**Apoorva Chawla** (Member, IEEE) received the B.Tech. degree in electronics and communication engineering from the Gautam Buddh Technical University, Greater Noida, India, in 2012, and the M.Tech. - Ph.D. dual degree in electrical engineering from the Indian Institute of Technology, Kanpur, India, in 2022. She is currently a Postdoctoral Researcher with the Department of Electronic Systems, Norwegian University of Science and Technology, Trondheim, Norway. Her research interests include sensor validation, Internet of Things, distributed detection, wireless communication, and signal processing. She was recipient of the TCS Research Fellowship for pursuing graduate studies with the Indian Institute of Technology, Kanpur, India. In 2019, she was selected as one of the finalists for the Qualcomm Innovation Fellowship by Qualcomm, India.

**Ferdinand Evert Uilhoorn** received the Ph.D. (*cum laude*) and D.Sc. degrees in gas engineering from the Warsaw University of Technology, Warsaw, Poland, in 2007 and 2017, respectively. He completed studies in the fields of mechanical and systems engineering with the Polytechnic Groningen and Delft University of Technology, Delft, The Netherlands, respectively. He is currently an Associate Professor with the Gas Engineering Group, Warsaw University of Technology. His research interests include single- and multiphase flow modeling, numerical methods, and data assimilation, with a focus on pipeline systems.

**Pierluigi Salvo Rossi** (Senior Member, IEEE) (Member, IEEE) was born in Naples, Italy, in 1977. He received the Dr.Eng. degree (*summa cum laude*) in telecommunications engineering and the Ph.D. degree in computer engineering from the University of Naples "Federico II", Naples, Italy, in 2002 and 2005, respectively. He is currently a Full Professor and the Deputy Head with the Department Electronic Systems, Norwegian University of Science and Technology (NTNU), Trondheim, Norway. He is also a part-time Research Scientist with the Department Gas Technology, SINTEF Energy Research, Norway. He was with the University of Naples "Federico II", Naples, Italy, with the Second University of Naples, Naples, Italy, with NTNU, Norway, and with Kongsberg Digital AS, Norway. He held visiting appointments with Drexel University, Philadelphia, PA, USA, Lund University, Lund, Sweden, NTNU, Norway, and Uppsala University, Uppsala, Sweden. His research interests include communication theory, data fusion, machine learning, and signal processing. Prof. Salvo Rossi was awarded as an Exemplary Senior Editor of the IEEE COMMUNICATIONS LETTERS in 2018. He is (or has been) in the Editorial Board of the IEEE OPEN JOURNAL OF THE COMMUNICATIONS SOCIETY, IEEE TRANSACTIONS ON SIGNAL AND INFORMATION PROCESSING OVER NETWORKS, IEEE SENSORS JOURNAL, IEEE COMMUNICATIONS LETTERS, and IEEE TRANSACTIONS ON WIRELESS COMMUNICATIONS.